1-1-2015

Microstructure evolution during isochronal annealing of a 42% cold rolled TRIP-TWIP steel

Sudipta Pramanik
University of Wollongong, sp345@uowmail.edu.au

Ahmed A. Saleh
University of Wollongong, asaleh@uow.edu.au

Dagoberto Brandao Santos
University Federal de Minas Gerais

Elena V. Pereloma
University of Wollongong, elenap@uow.edu.au

Azdiar A. Gazder
University of Wollongong, azdiar@uow.edu.au

Microstructure evolution during isochronal annealing of a 42% cold rolled TRIP-TWIP steel

Abstract

A high manganese TRIP-TWIP steel was cold rolled to 42% thickness reduction and isochronally annealed between 600 to 900 °C for 300 s. The microstructural evolution during annealing was studied by high resolution electron back-scattering diffraction. After cold rolling, the steel comprised predominant fraction of α'-martensite, a small fraction of blocky ε-martensite and a trace fraction of retained austenite (γ). During annealing, the reversion of ε and α' martensite to γ was followed by the recrystallisation of γ. While the processes of reversion to and recrystallisation of γ were completed by 700 °C, further annealing between 750 to 900 °C led to γ grain growth. A novel method to delineate the γ-γ grain boundaries was developed in order to accurately quantify γ grain size and subsequently the activation energy for γ grain growth.

Keywords

cold, twip, rolled, steel, trip, microstructure, evolution, during, isochronal, annealing, 42

Disciplines

Engineering | Science and Technology Studies

Publication Details

Pramanik, S., Saleh, A. A., Santos, D. B., Pereloma, E. V. & Gazder, A. A. (2015). Microstructure evolution during isochronal annealing of a 42% cold rolled TRIP-TWIP steel. IOP Conference Series: Materials Science and Engineering, 89 012042-1-012042-8.

Microstructure evolution during isochronal annealing of a 42% cold rolled TRIP-TWIP steel

S Pramanik[1,2*], A A Saleh[2], D B Santos[3], E V Pereloma[1,2] and A A Gazder[1]
[1]Electron Microscopy Centre, University of Wollongong, New South Wales 2500, Australia
[2]School of Mechanical, Materials and Mechatronic Engineering, University of Wollongong, New South Wales 2522, Australia
[3]Metallurgical and Materials Engineering Department, Federal University of Minas Gerais, Belo-Horizonte, Brazil

*Email: sp345@uowmail.edu.au

Abstract. A high manganese TRIP-TWIP steel was cold rolled to 42% thickness reduction and isochronally annealed between 600 to 900 °C for 300 s. The microstructural evolution during annealing was studied by high resolution electron back-scattering diffraction. After cold rolling, the steel comprised predominant fraction of α′-martensite, a small fraction of blocky ε-martensite and a trace fraction of retained austenite (γ). During annealing, the reversion of ε and α′ martensite to γ was followed by the recrystallisation of γ. While the processes of reversion to and recrystallisation of γ were completed by 700 °C, further annealing between 750 to 900 °C led to γ grain growth. A novel method to delineate the γ-γ grain boundaries was developed in order to accurately quantify γ grain size and subsequently the activation energy for γ grain growth.

1. Introduction

Stringent environmental and safety regulations has led steelmakers and downstream automotive industries to develop new grades of advanced high-strength steels (AHSS) that improve on fuel economy through savings in vehicle weight and provide greater passenger safety. The high mechanical strengths (>1100 MPa) and large ductilities (≥ 55%) of this family of AHSS steels is due to their capacity to work harden considerably to large imparted strain levels [1, 2]. AHSS steels containing 15-25 wt.% Mn along with 2-4 wt.% of Si and Al comprise a metastable face centred cubic (fcc) austenite (γ) phase that accommodates deformation via a combination of twinning (TWIP) and transformation (TRIP) induced plasticity effects. γ phase transforms to either hexagonal close packed (hcp) ε-martensite (γ → ε) or body centred cubic (bcc) α′-martensite. The latter can occur via two possible routes: γ → α′ or γ → ε → α′ [3].

Upon annealing, the reversion of deformation-induced ε and α′ martensite to γ occurs [4, 5]. Thereafter the γ undergoes recrystallisation which is manifested by the growth and polygonisation of γ grains. The process of γ recrystallisation is typically accompanied by the formation of annealing twins. With increasing annealing temperatures, thermally-induced ε and α′ martensites also manifest within recrystallised γ grains as parallel or intersecting ε plates with α′ martensite grains located between the ε martensite plates.

The driving force behind γ grain growth is an overall reduction of the total grain boundary area in order to reduce the total energy associated with grain boundaries [6]. The rate of grain growth is dictated

by boundary mobility and the activation energy for grain growth. In turn, boundary mobility depends on alloy composition, annealing temperature and the nature of the growing boundary. For example, the addition of alloying elements leads to an overall decrease in grain growth rate due to the solute drag effect [7], an increase in annealing temperature results in higher boundary mobility and coincident site lattice boundaries are less affected by the solute drag effect compared to other boundaries [8, 9]. The fundamental parameter controlling overall grain growth behaviour is the activation energy which is defined as the overall resistance of a material to grain growth. It follows that alloys with higher activation energy values compared to the pure metal returns a lower rate of grain growth.

The standard method to compute the activation energy for grain growth is by tracking the change in grain size with annealing time or temperature. In the present steel, γ grain sizes can be measured from optical and secondary electron micrographs or electron back-scattering diffraction (EBSD) maps. However, it is difficult to accurately distinguish the various phases using the former two methods. On the other hand, while EBSD successfully identifies all phases, the returned grain size information is based on a user-defined critical boundary misorientation angle that is uniformly applied to all phases. As a result, the γ grain size is markedly underestimated due to the inability to strictly define γ-γ boundaries. The latter is caused by the boundary contributions from thermally induced ε and α′ martensites (i.e. – the existence of γ-ε and γ-α′ martensite interphase boundaries). In turn, the underestimated γ grain sizes lead to the calculation of erroneous activation energy values. Thus a method is needed to accurately determine γ grain sizes by using γ-γ boundaries only.

With respect to the above outlook, the aim of this work is two-fold: (i) to characterise the evolution of the various phases during isochronal annealing and (ii) to quantify the activation energy for γ grain growth by accurately determining γ grain sizes from γ-γ boundaries only.

2. Experimental procedure

An Fe-17Mn-2Si-3Al-1Ni-0.06C wt.% steel was slab cast and homogenised at 1100 °C for 7200 s. The homogenised slab was hot-rolled at 1100 °C to 52.5% thickness reduction in 4 passes. Cold rolling of the hot-rolled strip was subsequently done to 42% thickness reduction in 11 passes. Samples were machined from the centre of the cold-rolled strip and isochronally annealed between 600 and 900 °C. Annealing involved a heating period of 240 s to the set temperature, a holding period of 300 s followed by immediate water quenching. Ø3 mm diameter discs were punched out from the normal direction (ND) -rolling direction (RD) mid-plane and twin-jet electropolished using a solution of 90% methanol and 10% perchloric acid in a Struers Tenupol-5 operating at 30 V (~150 mA) and -25 °C.

High resolution EBSD was undertaken on a JEOL JSM-7001F field emission gun - scanning electron microscope operating at 15 kV accelerating voltage, ~5.5 nA probe current, 12 mm working distance and equipped with a Nordlys-II(S) EBSD detector interfacing with the Oxford Instruments AZtec software suite. EBSD maps were acquired with step sizes of 30 nm for the cold-rolled and 600 °C annealed samples and 100 nm for the 700 to 900 °C annealed samples.

3. Analytical procedure

3.1 EBSD map post-processing

The raw EBSD maps of the 42% cold rolled and isochronally annealed samples returned an average indexing rates of 64.0% and 86.3±14.1%, respectively. Post-processing of the maps was undertaken using the Oxford Instruments Channel-5 software package using well-established procedures (see Ref. [10] and the references therein) by eliminating any potential wild orientation spikes and filling in zero solutions via cyclic extrapolation from 8 to 5 neighbours. As a consequence, the above procedure rules out the introduction of any artificial grains. In all the maps, (sub)grain structures are defined by a minimum of three pixels and are bound by misorientations (θ) ≥ 2°. Here 2° ≤ θ < 15° are classified as low angle grain boundaries (LAGBs) whereas $\theta \geq 15°$ denote high angle grain boundaries (HAGBs). First order twin boundaries (TB_γ) are defined as $\Sigma 3 = 60°$ <111> with a maximum deviation ($\Delta\theta$) of 6° following the Palumbo-Aust criterion ($\Delta\theta \leq 15° \Sigma^{-5/6}$) [11].

3.2 Boundary map image processing

The sample annealed at 900 °C is used to describe the procedure applied to identify the γ-γ grain boundaries and to calculate the γ grain sizes (Figure 1). It is pointed out that the methodology described in the following paragraphs relies on the image processing of grain boundary maps and does not utilise any orientation data.

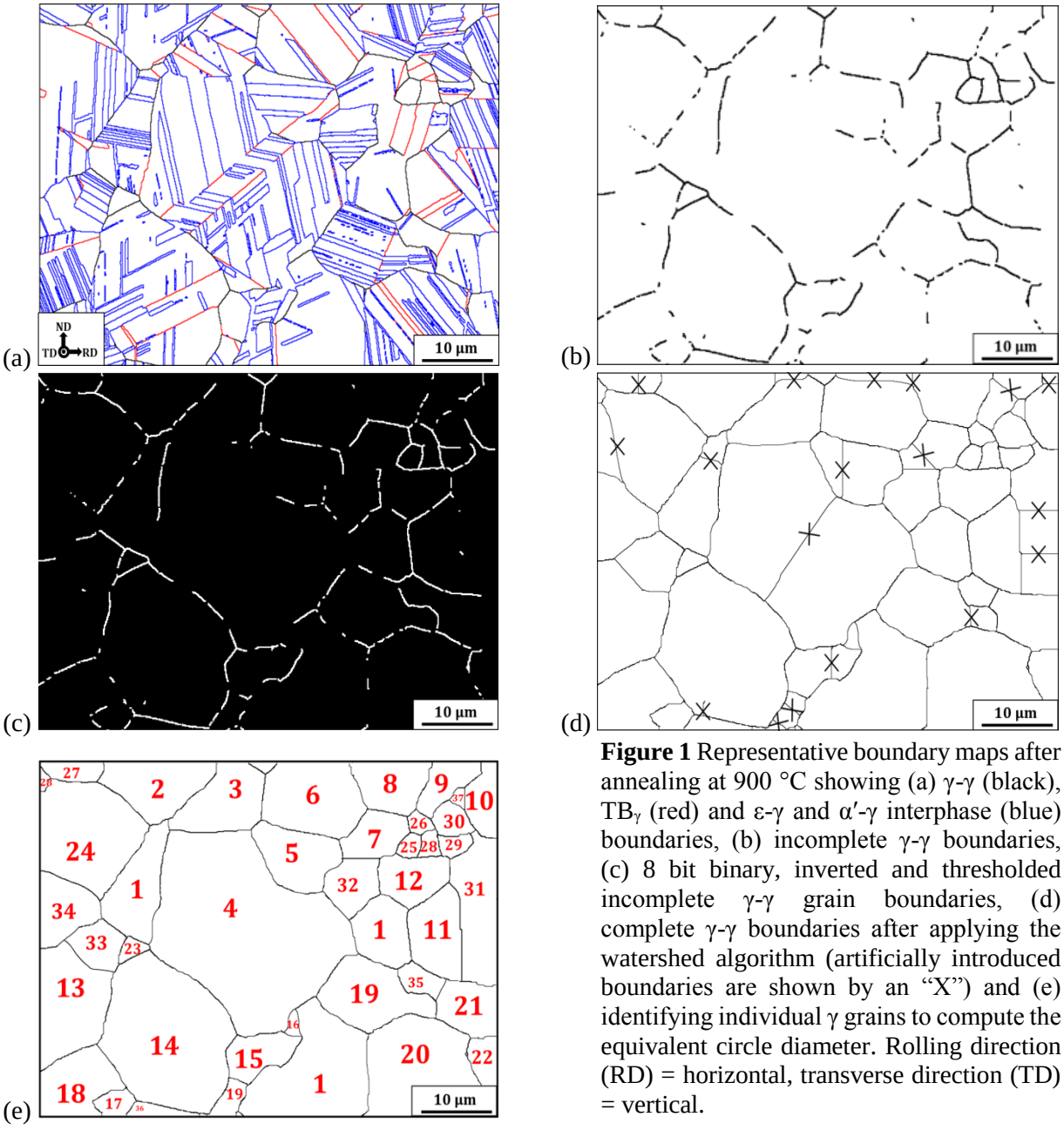

Figure 1 Representative boundary maps after annealing at 900 °C showing (a) γ-γ (black), TB_γ (red) and ε-γ and α′-γ interphase (blue) boundaries, (b) incomplete γ-γ boundaries, (c) 8 bit binary, inverted and thresholded incomplete γ-γ grain boundaries, (d) complete γ-γ boundaries after applying the watershed algorithm (artificially introduced boundaries are shown by an "X") and (e) identifying individual γ grains to compute the equivalent circle diameter. Rolling direction (RD) = horizontal, transverse direction (TD) = vertical.

As shown in Figure 1a, the procedure began by creating a map comprising γ-γ high-angle grain boundaries (black), 60° <111> twin boundaries of the γ phase (red) and ε-γ, α′-γ interphase boundaries (blue). Following this, the colour of the TB_γ and interphase boundaries was re-assigned to white in order to return the incomplete γ-γ grain boundary map (Figure 1b).

The incomplete γ-γ boundary map was saved as a TIFF image and imported into the ImageJ software package [12]. A pixel-based image scale was defined, then the image was cropped to remove legend information. The cropped RGB image was then converted to an 8 bit binary image and inverted such that the pixels comprising the incomplete γ-γ grain boundaries were white while the pixels denoting the γ grain interior were black (Figure 1c). The above procedure was necessary to reveal the incomplete γ-γ grain boundaries and to enable image thresholding into two distinct pixels sets of 0 (or black) and 255 (white) colour channels. Next, the watershed algorithm was applied to complete the γ-γ boundaries by connecting the end pixels of incomplete γ-γ boundaries to their nearest neighbouring pixels by the linear shortest distance (Figure 1d) [13].

Following this, Figures 1b and 1d were visually compared in order to manually remove any artificially introduced boundaries (see the boundaries marked with an "X" in Figure 1d). Once completed, the γ-γ grain boundary outlines were detected and the number of pixels within each outlined grain was quantified in order to determine the grain areas. The grain areas were then used to compute the equivalent circle diameter (ECD).

It follows that the ECD value corresponds to that diameter of a circle whose area is equivalent to the area of an γ grain [14]. Lastly, the average and standard deviation of the ECD distribution is computed and the procedure was repeated for all the annealing conditions (Figure 2).

3.3 Calculation of the activation energy

The activation energy for γ grain growth was calculated by using the equation given below [15]:

$$d_T^{1/N} - d_0^{1/N} = K_0 t^n e^{(-Q/RT)} \quad (1)$$

where d_T is the γ grain size (in microns) at a given annealing temperature T (in K), d_0 = 1.85±1.4 μm is the initial average γ grain size (determined at 700 °C), N is the grain growth exponent, K_0 is a kinetic constant that is equivalent to the y-intercept, t = 300 s is the holding time during annealing, n = 1 is a constant, Q is the computed activation energy for γ grain growth (in kJ/mol) and R = 8.314 J/molK is the universal gas constant.

The value for the grain growth exponent measured from a 1000 °C isothermal annealing experiment undertaken on an Fe-29Mn-5Al-0.06C TWIP steel was found to be N = 0.34 [15]. Due to the scarcity of data on high Mn steels, the change in N with homologous temperature ($T_h = T/T_m$ with T_m = 1550 °C) was estimated using data from austenitic stainless steel [16, 17]. Using N = 0.34 for $0.69T_h$, 1000 °C as a reference point [15], the extrapolated N-values for the $0.53T_h$ to $0.64T_h$ or 700 to 900 °C temperature range that corresponds to our isochronal annealing experiments varies between 0.29 and 0.33, respectively. Since abnormal grain growth is absent in the present steel, drastic changes to the N-value are not expected [17]. Consequently, N = 0.29 and 0.33 are used to estimate the range of activation energies for γ grain growth.

When using Eq. (1) it is also implied that: (i) grain morphology is equiaxed and the microstructure is of uniform size and (ii) no inclusions or chemical segregation are present at grain boundaries [18]. The activation energy (Q) is calculated from the slope of $\ln(d_T^{1/N} - d_0^{1/N})$ vs $1/T$ as shown in Figure 3b for N = 0.29.

4. Results and Discussion

4.1 Microstructural evolution during annealing

Figure 2a is a representative phase distribution map of the 42% cold rolled microstructure. It comprises large aspect ratio α′ martensite (green) grains along with blocky ε martensite (violet) and untransformed γ (grey) grains. It is self-evident that α′ martensite is the dominant phase followed by ε martensite and only a trace amount of untransformed γ. Gazder *et al.* [19] reported similar results for 66% cold rolled TRIP-TWIP steel. Annealing at 600 °C results in martensite reversion such that the map comprises a

dominant γ phase, a remanent α′ martensite phase and an absent ε martensite phase. The last observation suggests that ε martensite reverted to γ at temperatures lower than 600 °C [20].

Annealing at 700 °C results in the development of equiaxed γ grains with a large fraction of annealing twin boundaries and small fractions of thermally-induced ε and α′ martensites (Figure 2c). Further annealing between 750 to 900 °C leads to γ grain growth such that a wide distribution in γ grain sizes is noted (Figures 2c-g). The microstructures are a mix of fine γ grains located at the boundary triple junctions of the coarse γ grains. This is expected, considering that: (i) the concurrent processes of α′ martensite reversion and subsequent γ nucleation occur over a range of annealing temperatures and (ii) the growth of previously recrystallised γ grains (as a result of higher boundary mobilities across some interfaces) will also result in coarser γ grains in the microstructure.

The formation of thermally-induced ε and α′ martensites in relatively coarse γ grains after 750 to 900 °C annealing (Figures 2c-g) agrees with previous reports by Refs. [21] and [22]. The nucleation and growth of ε martensite plates was explained by Jiang *et al.* [21] on the basis of their increased probability of nucleating at the intersections of stacking faults in coarse γ grains. In the case of fine γ grain sizes (classified here as 5-15 μm), ε martensite comprises morphologically similarly-oriented plates propagating across entire grains (dashed white circle in Fig 1(g)) whereas in the case of coarse γ grains (>15 μm) (solid white circle in Fig 1(g)), a network of intersecting ε martensite plates is promoted. The above observation agrees with Takaki *et al.* [22] who also reported that ε martensite plates tend to propagate across smaller γ grains (<30 μm) or consists of intersecting plates in larger γ grains (>130 μm).

4.2 Activation energy for γ grain growth

To-date, conventional approaches to γ grain size calculations in the presence of microstructural features or secondary phases have tended to underestimate the average γ grain size. In the present steel, the underestimation is caused by the inclusion of TB_{γ}, γ-ε and γ-α′ martensite interphase boundaries when computing the γ grain size (white circles in Figure 3a). However, when twin and interphase boundaries are excluded and the γ-γ boundaries are strictly defined via the procedure detailed in Section 3.2, a more accurate measure of the γ grain size can be obtained (black circles in Figure 3a).

When the above grain sizes are used in conjunction with Eq. (1), the activation energies for γ grain growth can be computed (Figure 3b). When twin and interphase boundaries are considered and N = 0.29, the activation energy was estimated as 232.0±23.6 kJ/mol (white circles in Figure 3b). The relatively poor linear fit (R^2 = 0.80) results in a higher value of standard deviation in this case (±23.6 kJ/mol). Alternatively, when γ-γ boundaries are strictly delineated using the method described in Section 3.2, a more robust linear fit (R^2 = 0.99) results in an activation energy of 265.8±9.9 kJ/mol. In order to compute the possible range of activation energy, N = 0.33 ($0.64T_h$, 900 °C) was used while considering only γ-γ boundaries and an activation energy of 243.5±10.5 kJ/mol was estimated.

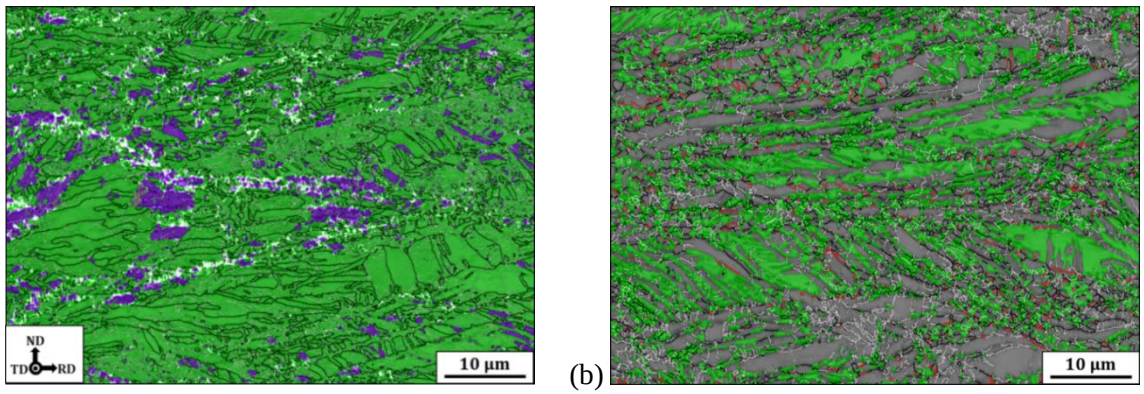

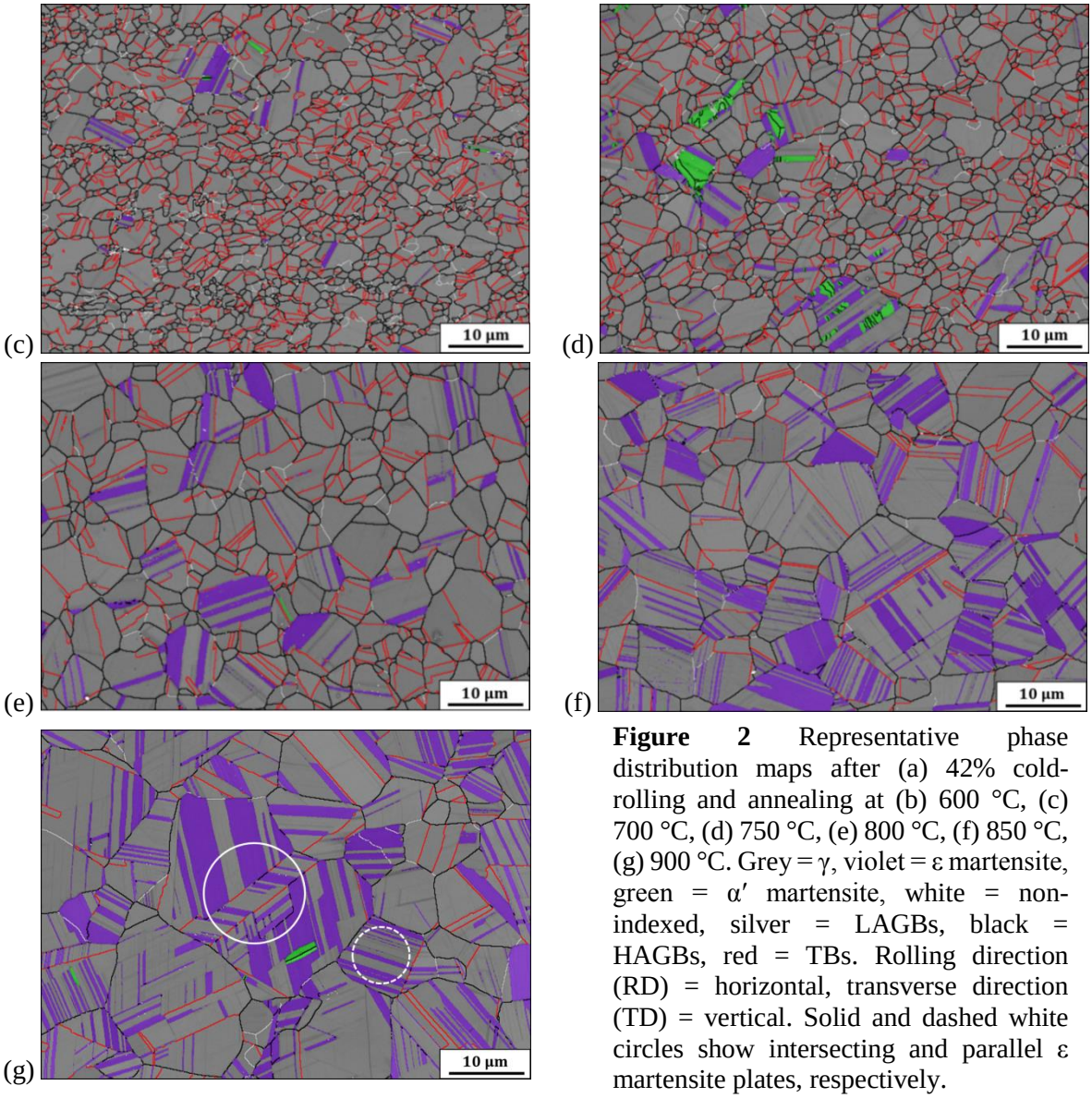

Figure 2 Representative phase distribution maps after (a) 42% cold-rolling and annealing at (b) 600 °C, (c) 700 °C, (d) 750 °C, (e) 800 °C, (f) 850 °C, (g) 900 °C. Grey = γ, violet = ε martensite, green = α′ martensite, white = non-indexed, silver = LAGBs, black = HAGBs, red = TBs. Rolling direction (RD) = horizontal, transverse direction (TD) = vertical. Solid and dashed white circles show intersecting and parallel ε martensite plates, respectively.

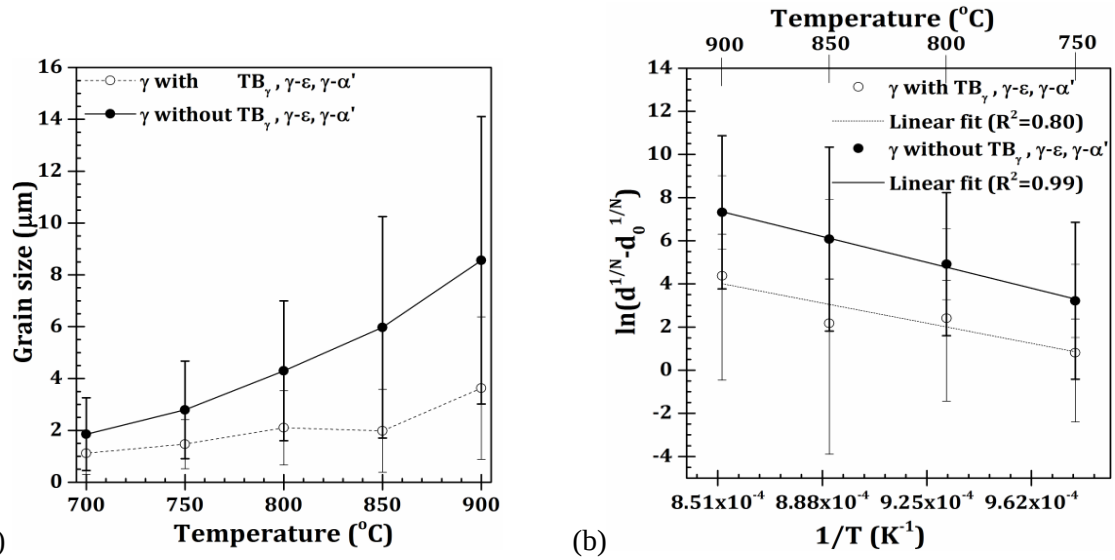

Figure 3 (a) Variation of γ grain size with annealing temperature and (b) the linear fit that computes the activation energy for γ grain growth using N = 0.29 when TB_{γ}, γ-ε and γ-α′ boundaries are included and excluded (white circles with thin dashed lines and black circles with thick solid lines, respectively).

The above calculated values can be compared to the activation energies determined from the γ grain size data of Refs. [23, 24]. For the Fe-18Mn [24] and Fe-18Mn-1.5Si-0.6C [23] steels, N values of 0.29 ($0.53T_h$, 700 °C) and 0.30 ($0.56T_h$, 750 °C) resulted in activation energy estimates of 283.83 and 263.4±11.7 kJ/mol, respectively. It follows that the activation energy for γ grain growth for this class of TRIP-TWIP steels is significantly higher than the activation energy for grain boundary diffusion in γ iron (Q_b = 149 kJ/mol) [25] and tends to be close to the self-diffusion of γ (Q_s = 270 kJ/mol) [5]. In turn, this indicates that lattice diffusion may be a key mechanism for γ grain growth rather than grain boundary diffusion.

5. Conclusions

The microstructural evolution of a TRIP-TWIP steel subjected to 42% cold-rolling and isochronal annealing in the temperature range from 600 to 900 °C for 300s was studied by high resolution electron back-scattering diffraction.

1. After cold rolling, the steel contained predominantly α′ martensite, a small fraction of blocky ε martensite and a trace amount of untransformed γ. Annealing resulted in the reverse transformation of ε and α′ martensites to γ, the subsequent recrystallisation and growth of γ and the development of annealing twins. Formation of thermally-induced ε and α′ martensites within recrystallised γ grains occurred on cooling.

2. A method to accurately determine the ECD-based grain size of recrystallised γ was developed. It involved the removal of twin and interphase boundaries and strictly defining γ-γ boundaries only. In turn, the γ grain sizes were used to compute the activation energy for γ grain growth. The computed activation energy of 265.8±9.9 kJ/mol indicates that lattice diffusion may be a key mechanism for γ grain growth.

Acknowledgements

The authors acknowledge the use of the JEOL–JSM7001F FEG-SEM purchased with the financial support from the Australian Research Council (LE0882613). This work was supported by the Engineering Materials Research Strength at UOW.

References

[1] Grässel O, Krüger L, Frommeyer G and Meyer L W 2000 *Int. J. Plast.* **16** 1391-409
[2] Frommeyer G, Brux U and Neumann P 2003 *ISIJ Int.* **43** 438-46
[3] Tomota Y, Strum M and Morris J W 1986 *Metall. Trans. A* **17** 537-47
[4] Lü Y, Hutchinson B, Molodov D A and Gottstein G 2010 *Acta Mater.* **58** 3079-90
[5] Lü Y, Molodov D A and Gottstein G 2011 *Acta Mater.* **59** 3229-43
[6] Huang Y and Humphreys F J 2012 *Mater. Chem. Phys.* **132** 166-74
[7] Suehiro M, Liu Z K and Ågren J 1996 *Acta Mater.* **44** 4241-51
[8] Simpson C J, Aust K T and Winegard W C 1971 *Metall. Trans.* **2** 987-91
[9] Aust K T and W R J 1959 *Trans. AIME* **125** 119-27
[10] Gazder A A, Al-Harbi F, Spanke H T, Mitchell D R and Pereloma E V 2014 *Ultramicrosc.* **147** 114-32
[11] Palumbo G and Aust K T 1990 *Acta Metall. Mater.* **38** 2343-52
[12] Schneider C A, Rasband W S and Eliceiri K W 2012 *Nat. Methods* **9** 671-5
[13] Pérez J M M and Pascau J 2013 *Image Processing with ImageJ* (Birmingham UK: Packt Publishing)
[14] Jennings B R and Parslow K 1988 *Proc. Roy. Lond.: Math. Phys. Eng. Sci.* **419** 137-49
[15] Razmpoosh M H, Zarei-Hanzaki A, Haghdadi N, Cho J H, Kim W J and Heshmati-Manesh S 2015 *Mater. Sci. Eng. A* **638** 5-14
[16] Hu H and Rath B B 1970 *Metall. Trans.* **1** 3181-4
[17] Mizera J, Wyrzykowski J W and Kurzydłowski K J 1988 *Mater. Sci. Eng. A* **104** 157-62
[18] Rajasekhara S, Karjalainen L P, Kyröläinen A and Ferreira P J 2008 Kinetics of grain growth in ultra-fine grained AISI 301LN stainless steel. In: *Proc. of 6th European Stainless Steel Conference*, ed Karjalainen P and Hertzman S (Helsinki, Finland) pp 511-7
[19] Gazder A A, Saleh A A, Nancarrow M J B, Mitchell D R G and Pereloma E V 2015 *Steel Res. Int.* **86** doi: 10.1002/srin.201500089
[20] Escobar D P, Dafé S S F and Santos D B 2014 *J. Mater. Res. Tech.* **4** 162-70
[21] Jiang B H, Sun L, Li R and Hsu T Y 1995 *Scr. Metall.* **33** 63-8
[22] Takaki S, Nakatsu H and Tokunaga Y 1993 *Mater. Trans. JIM* **34** 489-95
[23] Jo S Y, Han J, Kang J H, Kang S, Lee S and Lee Y K 2015 *J. Alloy Compd.* **627** 374-82
[24] Jun J H and Choi C S 1998 *Mater. Sci. Eng. A* **257** 353-6
[25] Medina S F and Quispe A 2001 *ISIJ Int.* **41** 774-81